Rev. Roum. Sci. Techn.– Électrotechn. et Énerg.
Vol. **63**, *2*, pp. 000–000, Bucarest, 2018

Automatique et ordinateurs

COMPARATIVE ANALYSIS OF ROBUST CONTROLLER BASED ON CLASSICAL PROPORTIONAL-INTEGRAL CONTROLLER APPROACH FOR POWER CONTROL OF WIND ENERGY SYSTEM

OUAMRI BACHIR[1], AHMED-FOITIH ZOUBIR[2]

Key words: Wind energy, Doubly-fed induction generator (DFIG), Vector control, Power control, Proportional-integral (PI) controller, RST controller, Sliding mode controller (SMC).

The connection of a wind generator to an electrical grid depends essentially on its ability to respond to changes in wind speed and the quality of the energy produced. This paper presents an analysis of the control techniques of a wind energy conversion system (WECS) based on a doubly-fed induction generator (DFIG). To do this, and in order to realize independent control of the statoric active and reactive powers of the DFIG, a control law is synthesized using three controllers: proportional-integral (PI), polynomial RST and sliding mode controller (SMC). Their performances in terms of power reference tracking, robustness to the parametric variations of the generator, sensitivity to perturbations and reaction to speed variations are compared and evaluated by simulation results.

1. INTRODUCTION

Today, wind energy has become an unavoidable global reality. This energy source has been developed considering the diversity of the exploitable zones, the relatively attractive cost and especially not emitting greenhouse gases.

Currently most wind systems are equipped with a doubly-fed induction generator (DFIG). This generator allows: a variable-speed electricity generation (± 30 % around the synchronous speed), which allows better the exploitation of wind resources for different wind conditions, the reduction of mechanical stresses and acoustical noise, the improvement of the power quality and the low cost [1].

Since the DFIG is non-linear in nature, its generated powers present a system with variables strongly coupled. It is subject to many constraints, such as the effects of parametric uncertainties (heating of resistances, saturation of inductances, etc.) and external disturbances (speed variation). These constraints could thus divert the system from its optimal functioning [2].

In order to remedy these various problems, we call to more robust and efficient control techniques. In this context, we have referred to the use of direct control technique of the active and reactive statoric powers based on robust algorithms.

Our choice is based on this technique because it presents a great technical simplicity and especially from the point of view implementation which uses fewer loops, therefore less calculation and also fewer sensors. The sensitivity of this conventional control to parametric variations, perturbations and modeling errors of the machine also motivates our choice to make an analysis and a comparison of the three regulators: integral-proportional (PI), RST controller and sliding mode controller (SMC) in order to improve its performances and its robustness and above all to regain its different advantages.

In this paper, we describe in first the wind energy conversion system (WECS). Then, we will present the synthesis of the three regulators: PI, RST and SMC. Finally, we will give an analysis and a comparison on the performances of these three regulators in terms of reference tracking, sensitivity to perturbations and robustness against to the DFIG's parameters variations.

2. DESCRIPTION AND MODELING OF WIND ENERGY CONVERSION SYSTEM

The wind energy conversion system shown in Fig. 1 consists of a wind turbine, a gearbox, a DFIG directly connected through the stator to the grid and supplied through the rotor by ac/dc and dc/ac converter.

2.1. WIND TURBINE MODEL

The wind turbine converts the aerodynamic energy to mechanical energy. The total aerodynamic power available to the wind turbine is given by [3]:

$$P_{aer} = \frac{1}{2}\rho S_v V^3, \quad (1)$$

where S_v is the area swept by the blades of the turbine [m^2], ρ is the air density [kg/m^3] and V is the wind speed [m/s].

Due to various losses in wind energy system, the power extracted from the turbine rotor is less than the incidental power. The extracted power is expressed by [3, 4]:

$$P_{tur} = \frac{1}{2}C_p(\lambda,\beta)\rho\pi R^2 V^3, \quad (2)$$

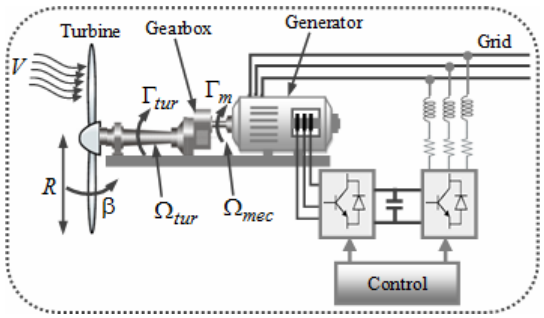

Fig. 1 – DFIG based Wind energy conversion system.

where R is the blade length [m], and C_p presents the aerodynamic efficiency of the turbine which is a function of both tip speed ratio λ, and blade pitch angle β[deg].

[1] Université de Bechar, Faculté de Technologie, Département de génie électrique, Bechar 08000 Algérie, E-mail: ouamribac@gmail.com
[2] Université des Sciences et de la Technologie d'Oran, Faculté de Génie Electrique, Département d'électronique, Oran 31000 Algérie

The power coefficient C_p and the tip speed ratio λ are given by:

$$\begin{cases} C_p = \dfrac{P_{tur}}{P_{aer}} \\ \lambda = \dfrac{R\Omega_{tur}}{V} \end{cases}. \tag{3}$$

The tip speed ratio λ and the power coefficient C_p are the dimensionless and so can be used to describe the performance of any size of wind turbine rotor. Figure 2 represents the power coefficient C_p as a function of λ and β.

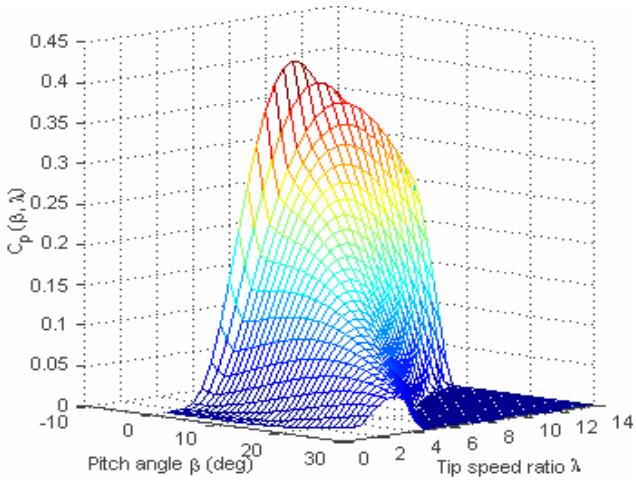

Fig. 2 – Power coefficient for the wind turbine model.

The gearbox adapts the slow turbine speed to the generator speed. This gearbox is modeled mathematically by the following equations [5, 6]:

$$\begin{cases} \Gamma_m = \Gamma_{tur}/G \\ \Omega_{tur} = \Omega_{mec}/G \\ J = (J_{tur}/G^2) + J_g \\ \Gamma_{tur} = P_{tur}/\Omega_{tur} \end{cases}, \tag{4}$$

where $\Omega_{tur}, \Omega_{mec}$ – the wind turbine speed and the generator shaft speed respectively[rpm], Γ_{tur} – aerodynamic torque, Γ_m – torque after gearbox (torque of the generator), G – gear ratio of the gearbox, J_g – inertia of the generator, J – total inertia that appears on the rotor of the generator, J_{tur} – inertia of the turbine.

The fundamental equation of the dynamics allows determining the evolution of the mechanical speed from the total mechanical torque (Γ_{mec}) applied to the rotor:

$$J\frac{d\Omega_{mec}}{dt} = \Gamma_{mec} = \Gamma_m - \Gamma_{em} - f\Omega_{mec}, \tag{5}$$

where Γ_{em} – electromagnetic torque, and f – is a viscous friction coefficient.

2.2. MATHEMATICAL MODEL OF THE DFIG

The simplified model of the DFIG, in a *d–q* reference frame can be represented by the expressions of stator, rotor voltages and flux components as follows [5]:

$$\begin{cases} v_{ds} = R_s i_{ds} + \dfrac{d\varphi_{ds}}{dt} - \omega_s \varphi_{qs} \\ v_{qs} = R_s i_{qs} + \dfrac{d\varphi_{qs}}{dt} + \omega_s \varphi_{ds} \\ v_{dr} = R_r i_{dr} + \dfrac{d\varphi_{dr}}{dt} - (\omega_s - \omega_r)\varphi_{qr} \\ v_{qr} = R_r i_{qr} + \dfrac{d\varphi_{qr}}{dt} + (\omega_s - \omega_r)\varphi_{dr} \\ \varphi_{ds} = L_s i_{ds} + M i_{dr} \\ \varphi_{qs} = L_s i_{qs} + M i_{qr} \\ \varphi_{dr} = L_r i_{dr} + M i_{ds} \\ \varphi_{qr} = L_r i_{qr} + M i_{qs} \end{cases}. \tag{6}$$

This electrical model is completed by the mechanical and the electromagnetic torques:

$$\begin{cases} \Gamma_m = \Gamma_{em} + J\dfrac{d\Omega}{dt} + f\Omega \\ \Gamma_{em} = P\dfrac{M}{L_s}(i_{qr}\varphi_{ds} - i_{dr}\varphi_{qs}) \end{cases}, \tag{7}$$

where R_s, R_r – per phase statoric and rotoric resistances, L_s, L_r – total cyclic statoric and rotoric inductances, M – magnetizing inductance, ω_s, ω_r – synchronous and rotor angular speeds, v_{ds}, v_{qs}, v_{dr}, v_{qr} – two-phase statoric and rotoric voltages, i_{ds}, i_{qs}, i_{dr}, i_{qr} – two-phase statoric and rotoric currents, φ_{ds}, φ_{qs}, φ_{dr}, φ_{qr} – two-phase statoric and rotoric fluxes, Ω – mechanical speed, P – pair pole number, J, f – inertia and viscous friction, Γ_m, Γ_e – mechanical and electromagnetic torques.

3. VECTOR CONTROL OF DFIG

To realize a statoric active and reactive power vector control, we choose a *d-q* reference-frame synchronized with the stator flux [5, 7]. By setting the statoric flux vector aligned with *d*-axis, we have: $\varphi_{ds} = \varphi_s$ and $\varphi_{qs} = 0$.

By supposing that the electrical supply network is stable, having for simple voltage V_s, that led to a stator flux φ_s constant. In addition, if the per phase stator resistance is neglected, which is a realistic approximation for medium and high power machines used in wind energy conversion, we obtain: $v_{ds} = 0$, $v_{qs} = V_s$ and $\varphi_s = V_s/\omega_s$. Hence, the active and reactive powers (P_s, Q_s) exchanged between the stator of the DFIG and the grid can be written versus rotoric currents as:

$$\begin{cases} P_s = v_{ds} i_{ds} + v_{qs} i_{qs} = -V_s \dfrac{M}{L_s} i_{qr} \\ Q_s = v_{qs} i_{ds} + v_{ds} i_{qs} = -V_s \dfrac{M}{L_s} i_{dr} + \dfrac{V_s^2}{L_s \omega_s} \end{cases}. \tag{8}$$

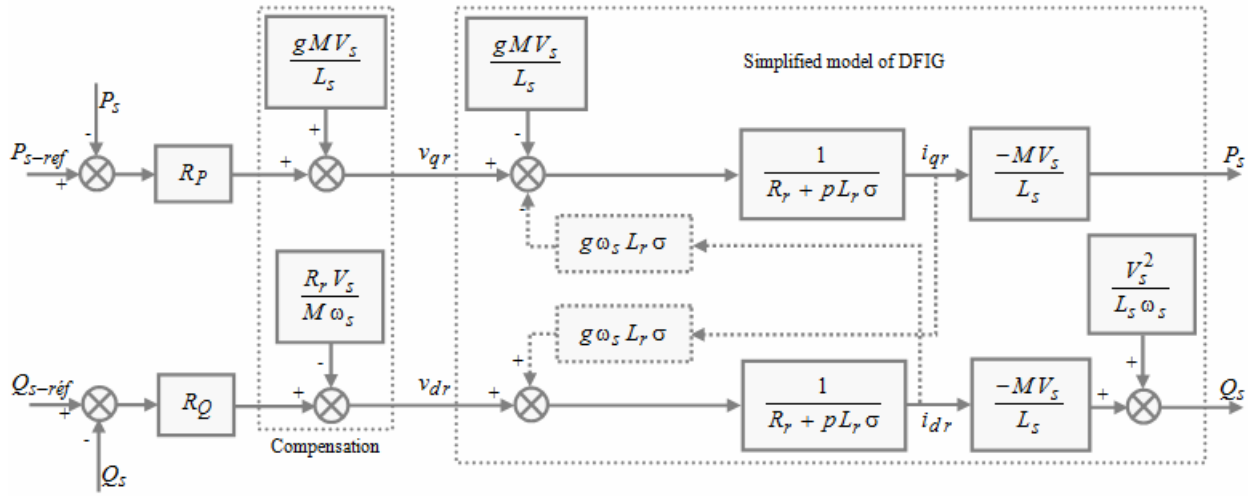

Fig. 3 – Global block-diagram of DFIG power control.

The rotoric voltages can be expressed by:

$$\begin{cases} v_{dr} = R_r i_{dr} + L_r \sigma \dfrac{\mathrm{d}i_{dr}}{\mathrm{d}t} - g\,\omega_s L_r \sigma i_{qr} \\ v_{qr} = R_r i_{qr} + L_r \sigma \dfrac{\mathrm{d}i_{qr}}{\mathrm{d}t} + g\,\omega_s L_r \sigma i_{dr} + g\dfrac{MV_s}{L_s} \end{cases}, \quad (9)$$

where $\sigma = \left(1 - (M^2/L_s L_r)\right)$ – is the leakage factor, $g = (\omega_s - \omega_r)/\omega_s$ – is the generator slip.

The used method in the power control consists to neglect the cross-coupling terms and to set up an independent regulator in each axis to control separately the active and reactive power. This method is called the direct control method because the power controllers directly control the rotoric voltages. The quadratic component of the rotor v_{qr} controls the active power (the electromagnetic torque) and the direct component v_{dr} controls the reactive power exchanged between the stator and the network.

Knowing equations (8) and (9), it is possible to synthesize the regulators and establish the global block-diagram of the controlled system (Fig. 3), where the blocks R_P and R_Q represent active and reactive power regulators. The aim of these regulators is to obtain high dynamic performances in terms of reference tracking, sensitivity to perturbations and parametric robustness. To realize these objectives, three types of regulators are studied, analysed and compared: proportional integral (PI), RST controller based on pole placement theory and sliding mode controller (SMC).

4. CONTROLLERS SYNTHESIS

In order to respect the context of the control based on the PI controller, from the point of view philosophy of linear regulators, we chose to study the control of DFIG in generator using three types of regulators. The PI will serve as a comparison reference since it's the most used and the simplest to synthesize. The results it gives in terms of a reference tracking, sensitivity to perturbations and robustness will be compared with those of an RST controller based on pole placement theory. We will see that the synthesis of this regulator allows taking into account a model of perturbation. Another type of controller with sliding mode (SMC) will be subject of a comparison with the PI. The sliding mode control takes into account the problems of stability and good performances in a way systematically in its approach. Its non-linear character makes its dynamics insensitive to modeling errors, to parametric variations and to external disturbances.

4.1. PI CONTROLLER SYNTHESIS

It is a simple and easy controller to implement. Figure 4 shows the bloc-diagram of the system implemented with this controller. In our case the transfer-function $(k_p + k_i/p)$ corresponds to R_P and R_Q regulators in Fig. 3. The terms of A and B are defined as follows:

$$A = L_s R_r + p L_s L_r \sigma \text{ and } B = MV_s . \quad (10)$$

The open-loop transfer-function (OLTF) integrating the presence of regulators is:

$$\text{OLTF} = = \frac{\left(p + \dfrac{k_i}{k_p}\right)}{\dfrac{p}{k_p}} \frac{\dfrac{MV_s}{L_s L_r \sigma}}{\left(p + \dfrac{L_s R_r}{L_s L_r \sigma}\right)} . \quad (11)$$

To eliminate the zero of the transfer-function, a pole-compensation method is used, such as:

$$\frac{k_i}{k_p} = \frac{R_r}{L_r \sigma} . \quad (12)$$

The open-loop transfer-function becomes:

$$\text{OLTF} = \frac{k_p \dfrac{MV_s}{L_s L_r \sigma}}{p} . \quad (13)$$

The closed-loop transfer-function (CLTF) is then expressed by:

$$\text{CLTF} = \frac{1}{1+\tau_r\, p}\ , \quad \text{where} \quad \tau_r = \frac{1}{k_p}\frac{L_s\, L_r\, \sigma}{M\, V_s}. \quad (14)$$

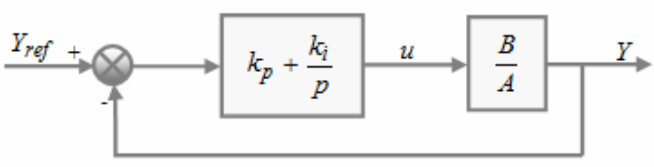

Fig. 4 – Bloc-diagram of the classical PI controller

The term τ_r refers the response time of the system which is fixed to the order of 10 ms. This value is sufficient for our application and a lower value might involve transients with important overshoots. The terms k_p and k_i are then expressed in terms of the response time and the parameters of the machine:

$$k_p = \frac{1}{\tau_r}\frac{L_s\, L_r\, \sigma}{M\, V_s}; \quad k_i = \frac{1}{\tau_r}\frac{R_r\, L_s}{M\, V_s}. \quad (15)$$

It is important to specify that the pole-compensation is not the only method to calculate a PI regulator but it is simple to elaborate with a first-order transfer-function and it is sufficient in our case to compare with other regulators.

4.2. RST CONTROLLER SYNTHESIS

The RST controller is a polynomial controller based on the robust pole placement architecture theory. It has the advantage of solving the tradeoff between rapidity and performance as compared to classical proportional integral PI controller [8].

Figure 5 shows the closed-loop of a system with its RST controller, where (B/A) is the transfer-function of the system, Y_{ref} is the reference disturbed by the variable β and R, S and T are the polynomials controller.

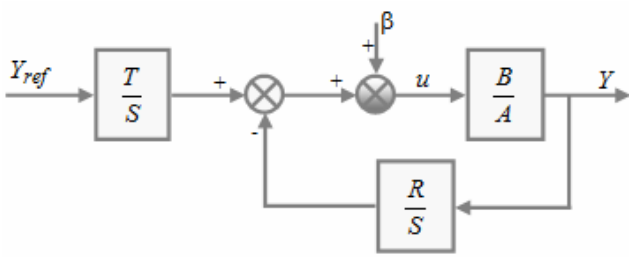

Fig. 5 – Structure of the RST controller.

In our case, terms A and B are expressed by:

$$\begin{cases} A = L_s\, R_r + p\, L_s\, L_r\, \sigma \\ B = M\, V_s \end{cases}, \quad (16)$$

where p is the Laplace operator.

The closed-loop transfer-function of the controlled system is:

$$Y = \frac{BT}{AS + BR} Y_{ref} + \frac{BS}{AS + BR}\beta. \quad (17)$$

The polynomials S and R appear in the denominator of (17) and their parameters are obtained by solving the Bezout equation defined by:

$$D = AS + BR = CF\ , \quad (18)$$

where C is the command polynomial and F is the filtering polynomial. In order to have good adjustment accuracy, we choose a strictly proper regulator. So if A is a polynomial of n degree $(\deg(A) = n)$ we must have:

$$\begin{cases} \deg(D) = \deg(A) + \deg(S) = 2n + 1 \\ \deg(S) = \deg(A) + 1 \\ \deg(R) = \deg(A) \end{cases}. \quad (19)$$

The polynomials of the proposed model can be written as:

$$\begin{cases} A = a_1\, p + a_0 \\ B = b_0 \\ D = d_3\, p^3 + d_2\, p^2 + d_1\, p + d_0 \\ R = r_1\, p + r_0 \\ S = s_2\, p^2 + s_1\, p + s_0 \end{cases}. \quad (20)$$

According to the robust pole placement method with T_c as control horizon and T_f as filtering horizon, the polynomial D (equation 18) is written as:

$$D = (p - p_c)(p - p_f)^2, \quad (21)$$

where $p_c = -1/T_c$ is the pole of polynomial C and $p_f = -1/T_f$ is the double pole of the polynomial filter F. The pole p_c must accelerate the system and is generally chosen three to five times greater than the pole p_a of A. p_f is generally chosen three times smaller than p_c. In our case we chose:

$$\begin{cases} p_c = 5\, p_a = -5\dfrac{R_r}{L_r\, \sigma} \\ T_f = \dfrac{1}{3} T_c \end{cases}. \quad (22)$$

From (21) and (22), we deduce the coefficients of polynomial D which are linked to the coefficients of S and R by the Sylvester matrix [8, 9]. Hence, we can deduce the parameters of the RST controller readily as:

$$\begin{cases} d_3 = a_1\, s_2 \rightarrow s_2 = \dfrac{d_3}{a_1} = \dfrac{1}{a_1} \\ d_2 = a_1\, s_1 \rightarrow s_1 = \dfrac{d_2}{a_1} = \dfrac{-(2\, p_f + p_c)}{a_1} \\ d_1 = a_0\, s_1 + b_0\, r_1 \rightarrow r_1 = \dfrac{(d_1 - a_0\, s_1)}{b_0} \\ \rightarrow r_1 = (p_f^2 + 2\, p_c\, p_f - a_0\, s_1)/b_0 \\ d_0 = b_0\, r_0 \rightarrow r_0 = \dfrac{d_0}{b_0} = \dfrac{-p_c\, p_f^2}{b_0} \end{cases}. \quad (23)$$

In order to determine the coefficients of T, we consider

that in steady state Y must be equal to Y_{ref} and as we know that $S(0)=0$, we conclude that $T(0)=R(0)$. In order to separate regulation and reference tracking, we try to make the term $(BT/(AS+BR))$ only dependent on C. We then consider $T=hF$ (where h is real) and we can write:

$$\frac{BT}{AS+BR}=\frac{BT}{D}=\frac{hB}{C}. \tag{24}$$

From equations (21), (23) and as $T(0)=R(0)$, we conclude that $h=R(0)/F(0)=r_0/p_f^2$.

Finally:

$$T=hF=\frac{r_0}{p_f^2}(p-p_f)^2. \tag{25}$$

4.3. SLIDING MODE CONTROLLER SYNTHESIS

The SMC is characterized by its simplicity of implementation, robustness against parametric variations and external disturbances affecting the system and few greedy in calculation time.

The basic principle of the sliding mode control consists to bring back the state trajectory to the sliding surface and to advance on it with a certain dynamic equilibrium point [10, 11, 12]. To design this controller three steps must be performed:

4.3.1. Choice of the sliding surface

For a nonlinear system presented in a canonical form:

$$\begin{cases}\dot{X}=f(X,t)+g(X,t)u(X,t)+d(t)\\ X\in\Re^n,\ u\in\Re^m,\ \text{rang}(g(X,t))=m\end{cases}, \tag{26}$$

where $f(X,t)$, $g(X,t)$ – are two continuous and uncertain non-linear functions assumed bounded, u – is the control input, and $d(t)$ – is the external disturbances.

We take the form of the general equation proposed by J. J. Slotine and Li to determine the slip surface given by:

$$\begin{cases}S(X)=\left(\frac{d}{dt}+\delta\right)^{n-1}e(X)\\ e(X)=X^d-X\end{cases}, \tag{27}$$

where e – is the error on the signal to be adjusted, δ - is a positive coefficient, n – is the system order, $X=[x,\dot{x},\ldots,x^{n-1}]^{\mathrm{T}}$ – is the state variable of the control signal, and $X^d=[x^d,\dot{x}^d,\ldots,x^{(n-1)d}]^{\mathrm{T}}$ – is the desired signal.

4.3.2. Convergence condition

The convergence condition is defined by the Lyapunov equation [13]; it makes the surface attractive and invariant.

$$S(X)\dot{S}(X)<0. \tag{28}$$

4.3.3. Control computation

The control algorithm is defined by the relationship:

$$u=u^{eq}+u^n, \tag{29}$$

where u – is the control signal, u^{eq} – is the equivalent control signal, u^n – is the switching controls term, and $\text{sign}(S(X))$ – is a sign function.

$$u^n=u^{\max}\,\text{sign}(S(X)), \tag{30}$$

where $u^{\max}$ – is positive gains, determine the ability of overcoming the chattering.

In order to reduce the chattering phenomenon due to the discontinuous nature of the controller, we replace the sign function by the saturation function as follows:

$$\begin{cases}u^n=u^{\max}\text{sat}(S(X)/\xi)\\ \text{sat}(S(X)/\xi)=\begin{cases}\text{sign}(S(X)) & \text{if } |S(X)|>\xi\\ S(X)/\xi & \text{if } |S(X)|<\xi\end{cases}\end{cases}. \tag{31}$$

4.4. CONTROL OF THE ACTIVE/REACTIVE POWER

In our study, we choose the error between the measured and references stator powers as sliding mode surfaces with $n=1$, so we can write the following expression:

$$\begin{cases}S(P)=P_{s-ref}-P_s\\ S(Q)=Q_{s-ref}-Q_s\end{cases}. \tag{32}$$

By deriving the surfaces with the replacement of the term of the powers P_s and Q_s (Eq. (8), then we shoot the expression of the current $\dot{i}_{qr}$ and $\dot{i}_{dr}$ from the equation of the voltage V_{qr} and V_{dr} respectively (Eq. (9)) the following is obtained:

$$\begin{cases}\dot{S}(P)=\dot{P}_{s-ref}+\frac{V_s M}{L_s L_r \sigma}(V_{qr}-R_r i_{qr})\\ \dot{S}(Q)=\dot{Q}_{s-ref}+\frac{V_s M}{L_s L_r \sigma}(V_{dr}-R_r i_{dr})\end{cases}. \tag{33}$$

By replacing the expression of V_{qr} and V_{dr} by $(V_{qr}^{eq}+V_{qr}^n)$ and $(V_{dr}^{eq}+V_{dr}^n)$ respectively, the control appears clearly in the following equations:

$$\begin{cases}\dot{S}(P)=\dot{P}_{s-ref}+\frac{V_s M}{L_s L_r \sigma}((V_{qr}^{eq}+V_{qr}^n)-R_r i_{qr})\\ \dot{S}(Q)=\dot{Q}_{s-ref}+\frac{V_s M}{L_s L_r \sigma}(V_{dr}^{eq}+V_{dr}^n)-R_r i_{dr})\end{cases}. \tag{34}$$

During the sliding mode and in steady state, the values of the sliding surface, the derivative of the sliding surface, and the switching control are:

$$S(P)=S(Q)=0,\ \dot{S}(P)=\dot{S}(Q)=0,\ V_{qr}^n=V_{dr}^n=0. \tag{35}$$

The equivalent controls are found from equation (34) and

written as follows:

$$\begin{cases} V_{qr}^{eq} = -\dot{P}_{s-ref}\dfrac{L_s L_r \sigma}{V_s M} + R_r i_{qr} \\ V_{dr}^{eq} = -\dot{Q}_{s-ref}\dfrac{L_s L_r \sigma}{V_s M} + R_r i_{dr} \end{cases}. \quad (36)$$

During the convergence mode, so that the condition $S(X)\dot{S}(X) \le 0$ is verified, the following is set:

$$\begin{cases} \dot{S}(P) = -\dfrac{V_s M}{L_s L_r \sigma} V_{qr}^{n} \\ \dot{S}(Q) = -\dfrac{V_s M}{L_s L_r \sigma} V_{dr}^{n} \end{cases}. \quad (37)$$

Consequently, the switching terms are given by the following:

$$\begin{cases} V_{qr}^{n} = KV_{qr}\,\mathrm{sat}(S(P)) \\ V_{dr}^{n} = KV_{dr}\,\mathrm{sat}(S(Q)) \end{cases}. \quad (38)$$

To verify the system stability condition, parameters KV_{qr} and KVd_{qr} must be positive.

To reduce any possible overshoot of reference voltages V_{qr} and V_{dr}, it is often useful to add voltage limiters which are expressed by:

$$\begin{cases} V_{qr}^{\lim} = V_{qr}^{\max}\,\mathrm{sat}(P) \\ V_{dr}^{\lim} = V_{dr}^{\max}\,\mathrm{sat}(Q) \end{cases}. \quad (39)$$

5. SIMULATION RESULTS AND DISCUSSIONS

In order to test and compare efficiently the proposed controllers, simulations investigated with a 10 kW generator connected to a 230 V/50 Hz grid. The machine's parameters are given in appendix.

The controller's performances are analysed and compared in three different configurations: reference tracking, sensitivity to the speed variation (perturbations) and robustness against parameters variations.

5.1. REFERENCE TRACKING

In order to observe the behavior in reference tracking, we have submitted our generator to active and reactive power steps. The DFIG is considered as working over ideal conditions mode (no perturbations and no parameters variations) and driven to its nominal value speed. Dynamic responses obtained respectively with the PI, RST and SMC controller are illustrated in Fig. 6.

From the results of the Fig. 6, it's clear that the measured active and reactive powers, for the three regulators, follow their references with static errors practically nil, but with a better transient response time in the case of the SMC. In this test, the decoupling between the two active and reactive powers is very remarkable and consequently, we can consider that these controllers present good static and dynamic performances.

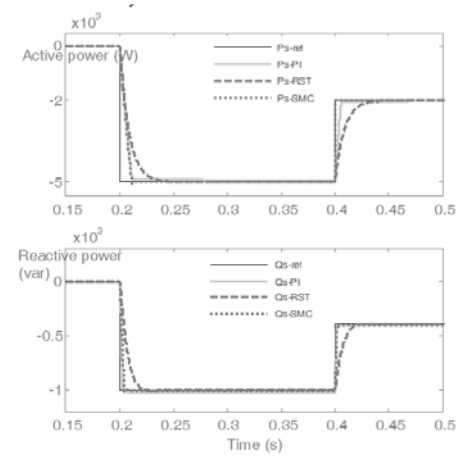

Fig. 6 – Response to the active and reactive power without parametric variations (reference tracking test).

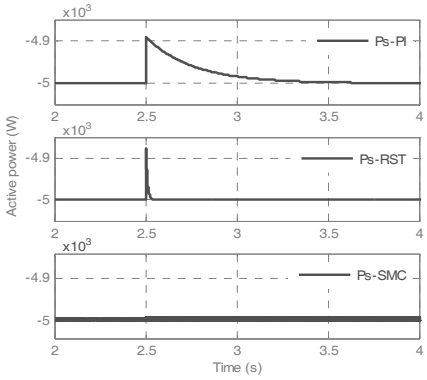

Fig. 7 – Response to a speed variation (Sensitivity test).

5.2. SENSITIVITY TO PERTURBATIONS

The objective of this test is to verify to what extent the measured powers remain at their set value when the speed rotation of the machine varies suddenly. In this case, the generator is driven at 1 320 rpm with constant references of active and reactive powers of –5kW and 500 var respectively. At time t = 2.5 s, the speed was suddenly varied from 1320 to 1 420 rpm.

Figure 7 shows the influence of this speed variation on the behavior of the powers generated for the three regulators.

The results of Fig. 7 show clearly the limits of the proportional-integral (PI) controller. Indeed, the synthesis of this one is based solely on the transfer-functions and none taken into account disturbances is foreseen. The powers measurements then show an important establishment time for the disturbance rejection. The RST controller integrates in its synthesis, the possible appearance of disturbances and therefore rejects more effectively the effects of speed variation. This is interpreted by the establishment time and of return to the initial state weaker. In the case of the sliding mode controller (SMC), the effect of this speed variation is practically negligible. It has better performances compared to the PI and RST controllers. Its non-linear behavior makes it insensitive to any external disturbance.

5.3. ROBUSTNESS TESTS

In order to investigate the robustness of the three controllers, the value of the rotoric inductance L_r and the magnetizing

inductance M are increased by 50% and 10% successively of their nominal values, the rotoric resistance R_r is doubled of its nominal value. The generator is running at its nominal speed.

Figure 8 shows the effect of parameters variation simultaneously on the active and reactive power responses for the three controllers.

The results of Fig. 8 show that in the case of the PI regulator, the time response is strongly modified whereas it remains unchanged when the RST and SMC controllers are used. In terms of rapidity, the SMC present a better response time compared to the RST controller.

6. CONCLUSION

This paper has introduced a wind energy conversion system based on a doubly fed induction generator connected to the grid. An appropriate model of the DFIG in a *d-q* axis has been established. In order to control independently statoric active and reactive power exchanged between the DFIG and the grid, a vector-control strategy has been presented. The synthesis of the PI, RST and SMC controllers has been detailed.

Simulations results have shown that performances are equivalent for the three controllers under ideal conditions. When the disturbance is presented (speed variation), the PI controller present its limits, the RST controller is more efficient and the SMC controller has better performances compared to the PI and RST controllers.

The direct control method based on the sliding mode controllers, compared to that based on the classical PI and the polynomial RST controllers, shows its best qualities in terms of: robustness to the parametric variations of the DFIG, rejection of disturbances, improvement of the rapidity and overshoot.

With the SMC controller, we were able to regain all the qualities of the classical direct control technique from the point of view: simplicity of implementation, minimum calculation time, number of sensors used reduced and moreover this regulation presents a control algorithm easily implantable in calculator. This ensures, therefore, a better quality of the electrical energy produced.

Appendix

Parameters of the DFIG used in simulation: 10 kW, $V_s = 230/400$ V, $f_s = 50$ Hz, $I_s = 20 / 30$ A, $P = 2$, $\Omega = 1\,420$ rpm, $R_s = 0.455\ \Omega$, $R_r = 0.19\ \Omega$, $L_s = 0.07$ H, $L_r = 0.0213$ H, $M = 0.034$ H, $f = 0.00114$ Nm/s, $J = 0.031$ Kgm^2.

Table 1

Parameters of the regulators

Regulator	Parameters
PI (gains)	$k_p = 0.05,\ k_i = 0.2$
RST (polynomial)	$R = [0.0444\ \ 4.8614] * 1e+7$ $S = [0.0003\ \ 1.0903\ \ 0.0003] * 1e+7$ $T = [0\ \ 0.0054\ \ 4.8614] * 1e+7$
SMC (gains)	$KV_{qr} = KV_{dr} = 48$
Value of Saturation	± 100
Fixed-step size	$1e-4$

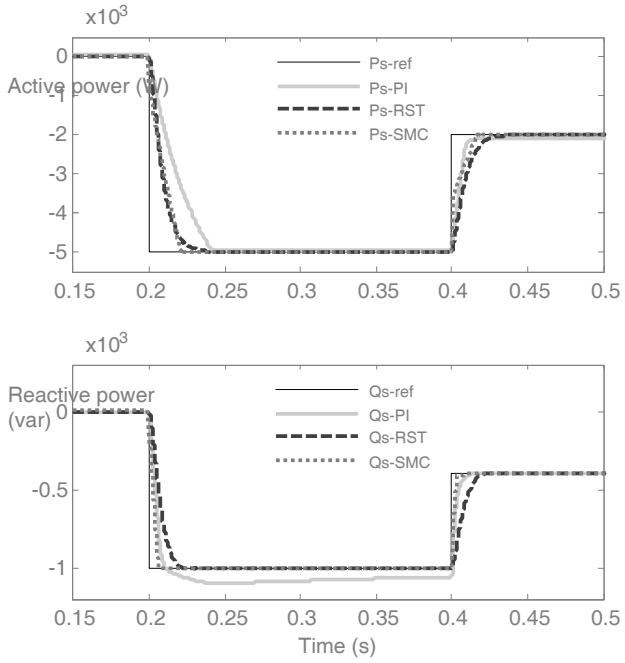

Fig. 8 – Response to the active and reactive power with simultaneously parametric variations ($L_r + 50\%$, $M + 10\%$, $R_r + 100\%$).

Received on January 28, 2017

REFERENCES

1. B. Wu, Y. Lang, N. Zargari, S. Kouro, *Power Conversion and Control of Wind Energy Systems*, John Wiley & Sons, Inc., USA, 2011.
2. F. Poitiers, T. Bouaouiche, M. Machmoum, *Advanced Control of a Doubly-Fed Induction Generator for Wind Energy Conversion*, Electric Power Systems Research, **79**, *7*, pp. 1085–1096, 2009.
3. E. Bossanyi, *Wind Energy Handbook*, John Wiley & Sons, New York, 2000.
4. D. Seyoum, C. Grantham, *Terminal Voltage Control of a Wind Turbine Driven Isolated Induction Generator using Stator Oriented Field Control*. IEEE, Transactions on Industry Applications, pp. 846–852, September 2003.
5. F. Poitiers, *Etude et commande de génératrices asynchrones pour l'utilisation de l'énergie éolienne, Machine asynchrone à cage autonome; Machine asynchrone à double alimentation reliée au réseau*, Thèse de doctorat de l'Ecole Polytechnique de l'Université de Nantes, 2003.
6. E.S. Abdin, W. Xu, *Control design and Dynamic Performance Analysis of a Wind Turbine Induction Generator Unit*, IEEE Trans. on Energy Conversion, **15**, *1*, March 2000.
7. A. Boyette, *Contrôle et commande d'un générateur asynchrone à double alimentation avec un système de stockage pour la production éolienne*, Thèse de doctorat de l'Université Henri Poincaré, Nancy I, 2006.
8. P. De Larminat, *Automatique, Commande des systèmes linéaires*, Seconde Edition, Paris, Hermès, 1996.
9. F. Hachicha, L. Krichen, *Performance analysis of a wind energy conversion system based on a doubly-fed induction generator*, IEEE, 8th International Multi-Conference on Systems, Signals & Devices, pp. 978–984, 2011.
10. J.J.E. Slotine, W.Li, *Applied nonlinear control*, Prentice-Hall, Inc., USA, 1998.
11. S. Müller, *Doubly fed induction generator systems*, IEEE Industry Applications Magazine, **08**, *3*, pp. 26–33, 2002.
12. V.I. Utkin, *Sliding mode control design principles and applications to electric drives*. IEEE Trans. Ind. Electronics, **40**, *1*, pp. 23–36, 1993.
13. P. Lopez, A.S. Nouri, *Théorie Elémentaire et pratique de la commande par les régimes glissants*, Springer-Verlag Berlin, Germany, 2006.